



A novel electrospun-aligned nanoyarn-reinforced nanofibrous scaffold for tendon tissue engineering



Chengwei Yang^{a,b,1}, Guoying Deng^{a,1}, Weiming Chen^c, Xiaojian Ye^{a,*}, Xiumei Mo^{c,**}

^a Department of Orthopaedics, Changzheng Hospital affiliated with Second Military Medical University, 415 Fengyang Road, Shanghai 200003, PR China

^b Department of Spinal Surgery, Lanzhou General Hospital of Lanzhou Military Command Region, 333 Nanbinhe Road, Lanzhou 730050, PR China

^c College of Chemistry, Chemical Engineering and Biotechnology, Donghua University, 2999 Renmin Road North, Songjiang District, Shanghai 201620, PR China

ARTICLE INFO

Article history:

Received 20 March 2014

Received in revised form 23 June 2014

Accepted 25 June 2014

Available online 2 July 2014

Keywords:

Electrospinning

Nanoyarn

Three-dimensional scaffold

Cell infiltration

Tendon tissue engineering

ABSTRACT

An electrospun-aligned nanoyarn-reinforced nanofibrous scaffold (NRS) was developed for tendon tissue engineering to improve mechanical strength and cell infiltration. The novel scaffold composed of aligned nanoyarns and random nanofibers was fabricated via electrospinning using a two-collector system. The aim of the present study was to investigate three different types of electrospun scaffolds (random nanofibrous scaffold, aligned nanofibrous scaffold and NRS) based on silk fibroin (SF) and poly(L-lactide-co-caprolactone) blends. Morphological analysis demonstrated that the NRS composed of aligned nanoyarns and randomly distributed nanofibers formed a 3D microstructure with relatively large pore sizes and high porosity. Biocompatibility analysis revealed that bone marrow-derived mesenchymal stem cells exhibited a higher proliferation rate when cultured on the NRS compared with the other scaffolds. The mechanical testing results indicated that the tensile properties of the NRS were reinforced in the direction parallel to the nanoyarns and satisfied the mechanical requirements for tendon repair. In addition, cell infiltration was significantly enhanced on the NRS. In conclusion, with its improved porosity and appropriate mechanical properties, the developed NRS shows promise for tendon tissue engineering applications.

© 2014 Elsevier B.V. All rights reserved.

1. Introduction

Tendons are composed of highly oriented collagen fibers and bear large loads in vivo. Compared with most other tissue types, tendons have relatively poor healing capacities, and damage to tendons frequently results in a failure to heal or the formation biomechanically inferior tissues. Ideal tissue-engineered functional replacements for damaged tendons would support both neo-tissue formation and the restoration of biomechanical function. In combination with cells, biological materials such as scaffolds play a decisive role in tendon tissue engineering. These scaffolds commonly

provide a synthetic extracellular matrix (ECM) environment and a three-dimensional (3D) template for tissue regeneration [1].

Electrospinning is an efficient and economical method to prepare scaffolds for tissue engineering applications [2]. Nanofibers fabricated via electrospinning are similar in size to the elements of the native ECM [3]. Microscale and nanoscale fibers improve cell proliferation and elicit superior metabolic and matrix forming activities [4,5]. Electrospun nanofibrous scaffolds have been applied to engineer various musculoskeletal tissues, including bone, cartilage, tendon, ligament, meniscus and annulus fibrosus tissues [6,7].

In a typical electrospinning process, electrospun polymer nanofibers are collected on a stationary grounded plate to form randomly oriented mats. The random nanofibrous scaffolds exhibit isotropic mechanical properties that are suitable for certain tissue engineering applications, such as wound dressings and drug delivery materials [8,9]. However, tendons that bear large mechanical loads along a restricted direction exhibit anisotropic mechanical properties. Highly organized collagen fibers in the ECM are critical for the mechanical function of tendons. Methods have been devised to induce the alignment of electrospun fibers in nanofibrous

* Corresponding authors at: Department of Orthopaedics, Changzheng Hospital affiliated with Second Military Medical University, 415 Fengyang Road, Shanghai 200003, PR China. Tel.: +8602181885624.

** Corresponding authors at: College of Chemistry, Chemical Engineering and Biotechnology, Donghua University, 2999 Renmin Road North, Songjiang District, Shanghai 201620, PR China, Tel: +8602167792653.

E-mail addresses: xjye2012@gmail.com (X. Ye), xmm@dhu.edu.cn (X. Mo).

¹ Chengwei Yang and Guoying Deng contributed equally to this work.

scaffolds to mimic the ultrastructure of the aligned collagen fibers. The most common method for generating aligned fibers is to collect fibers on a rapidly rotating mandrel. Li [10] demonstrated that aligned nanofibrous scaffolds could recapitulate anisotropic mechanical properties and direct cell adhesion. Furthermore, Baker [11] noted that the ability of cells to infiltrate nanofibrous scaffolds is limited due to the tightly packed nanofibers and small pore size. To address this limitation, a number of methodologies for improving cell infiltration have been investigated [9,11–13].

In the present study, a new method was developed to create aligned nanoyarn-reinforced nanofibrous scaffolds (NRSs) that mimic the structural and mechanical anisotropic properties of tendons. This novel 3D scaffold composed of aligned nanoyarns and random nanofibers was fabricated via electrospinning using a two-collector system. Due to its excellent mechanical properties and biodegradability [14], poly(L-lactide-co-caprolactone) (P(LLA-CL)) is often applied in tissue-engineered tendon scaffolds [15]. However, a substantial disadvantage of synthetic materials is the lack of natural cell recognition sites. Silk fibroin (SF), a natural biological protein, has favorable biocompatibility, hydrophilicity and low immunogenicity [16]. The electrospinning of SF/P(LLA-CL) blends yields a combined scaffold with superior biological and mechanical properties [5].

In this study, we used SF/P(LLA-CL) to fabricate the scaffolds and typical electrospinning methods to fabricate random and aligned nanofibrous scaffolds as controls. In addition, we characterized the organization and mechanical properties of these scaffolds and evaluated cell proliferation and infiltration in them. The results indicate that the aligned NRS is a viable option for use in tendon tissue engineering.

2. Materials and methods

2.1. Materials

Poly(L-lactide-co-caprolactone) (P(LLA-CL)) (LA:CL = 75:25; M_w : 340,000) was provided by GUNZE Co., Ltd. (Kyoto, Japan). *Bombyx mori* silkworm cocoons were kindly supplied by Jiaying Silk Co., Ltd. (Jiaying, China). 1,1,1,3,3,3-Hexafluoro-2-propanol (HFIP) was purchased from DaRui Co., Ltd. (Shanghai, China). P(LLA-CL) and HFIP were used without further purification.

2.2. Preparation of regenerated SF

Raw silk was degummed three times (30 min each) in 0.5% (w/w) Na_2CO_3 solution at 100 °C and washed with distilled water. The degummed silk was dissolved in a ternary $\text{CaCl}_2/\text{H}_2\text{O}/\text{EtOH}$ solvent system (1/8/2 molar ratio) for 1 h at 70 °C. After dialysis in a cellulose tubular membrane (250-7u; Sigma, USA) against distilled water for 3 days at room temperature, the SF solution was filtered and lyophilized to obtain regenerated SF sponges.

2.3. Scaffold fabrication

NRSs were manufactured by electrospinning using the modified two-collector system described by Lotus [17]. Our electrospinning setup is shown in Fig. 1. The setup includes two rotating collectors: a rotating hollow funnel and a rotating metal mandrel supported on a linear guide slider. In this experiment, the SF/P(LLA-CL) blend (weight ratio: 10:90) was dissolved in HFIP at 9 w/v%.

Electrospinning was performed between two rotating collectors placed approximately 10 cm apart horizontally to each other, as shown in Fig. 1. One collector was a 9-cm-diameter hollow metal funnel attached to the end of a 7-mm-diameter, 15-cm-long metal tube. The outer surface of the metal tube and all surfaces of the funnel, with the exception of a 2-mm band at the edge of the

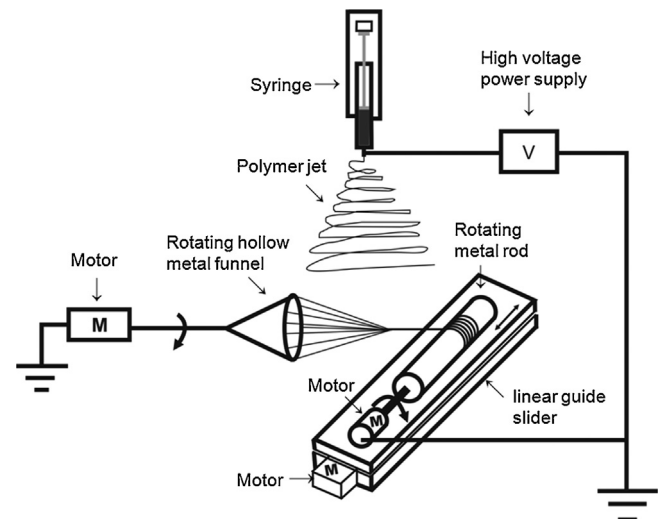


Fig. 1. Schematic illustration of the two-collector electrospinning system for fabricating the aligned nanoyarn-reinforced nanofibrous scaffold.

funnel, were covered with insulating tape to increase the probability of electrospinning jet deposition at the edge of the funnel. The second collector was a 5-cm-diameter, 6-cm-long metal mandrel supported on a linear guide slider. The SF/P(LLA-CL) blend solution was prepared and loaded into a syringe with a nozzle located vertically above the two grounded collectors at a distance of approximately 15 cm. During the electrospinning process, a voltage of 12 kV was applied to the nozzle, and the solution jet impelling rate was set at 1.2 mL/h. The electrospun fibers were collected between the two collectors. The hollow metal funnel was rotated at 500 rpm to twist the fibers together. The twisted yarns and untwisted fibers were continuously collected by the rotating mandrel at a rotation rate of 4 rpm. The mandrel collector moved back and forth on the linear guide slider in a horizontal direction following a set procedure (displacement distance: 3 cm; movement speed: 5 mm/min). After continuously collecting fibers for 12 h, an aligned nanoyarn-reinforced nanofibrous scaffold (NRS) with a thickness of approximately 600 μm was produced.

To fabricate the random nanofibrous scaffolds, a SF/P(LLA-CL) blend solution was prepared and loaded into a syringe, as described for the electrospinning of NRS. The solution was charged with a voltage of 12 kV and fed at a rate of 1.2 mL/h using a syringe pump. The electrospun random nanofibers were deposited on a grounded solid plate located at a distance of 15 cm from the blunt tip of the nozzle. When an aligned nanofibrous scaffold was fabricated, the flat fabric was replaced by a rotating target to collect the nanofibers 15 cm from the blunt tip. The speed of the rotating target was 8.3 m/s. After 8 h, random and aligned nanofibrous scaffolds with a thickness of approximately 300 μm were created.

2.4. Morphological characterization of the scaffolds

The surface morphologies of the scaffolds were examined using a scanning electron microscope (SEM; JSM-5600, JEOL, Japan). Before scanning, platinum was coated on the surface of the scaffolds twice for 10 s. To investigate the 3D structure, the scaffolds were embedded in epoxy resin, and cross-sectional ultrathin slices (approximately 80 nm) were obtained using an ultramicrotome (EM UC7, Leica, Germany). The cross-sectional microstructures of the specimens were examined using a transmission electron microscope (TEM; Tecnai G2 Spirit BioTWIN, FEI, USA) operated at 80 kV. The fiber diameter, nanoyarn bundle diameter and angle distribution (relative to the vertical axis) of the specimens ($n=3$) were

determined from the SEM images using ImageJ 1.47 (National Institutes of Health, USA). The angle distribution and mean diameter were determined from more than 100 randomly selected nanofibers and nanoyarns in the SEM images. The orientation of the fiber (or yarn) was determined by measuring the angle between the fiber (or yarn) and the direction of mandrel rotation for the aligned nanofibrous scaffolds and NRSs. The mean pore size was determined from more than 100 pores in the SEM images. A pore was identified as a void space surrounded by fibers (or yarns) on all sides and near the same depth in the SEM images. The porosity of the scaffolds was calculated using a previously described method [13] ($n=4$).

2.5. Uniaxial mechanical properties

After measuring the cross-sectional areas using a caliper, scaffold samples were cut into 5 mm × 20 mm rectangular samples, which were clamped with serrated grips and loaded onto an optical microscope and digital image correlation testing device [18]. The gauge length was determined using an optical microscope. The mechanical testing protocol was based on the previous literature [4]. Tensile tests were performed using a constant crosshead speed of 3 mm/min until failure. Strain was determined as extension normalized to the gauge length; stress was computed as the load normalized to the initial cross-sectional area. Young's modulus was computed as the slope of the stress–strain plot, determined by regression of the linear portion of the curve. The tensile strength and elongation at break were determined from the maximum stress and maximum strain before material failure ($n=5$).

2.6. Culturing and seeding of MSCs

Primary bone marrow-derived mesenchymal stem cells (MSCs) from Sprague-Dawley rats were harvested and cultured using a previously described protocol [19] approved by the Institutional Animal Care and Use Committee of Second Military Medical University (Shanghai, China).

Briefly, femurs that had been stripped of the adherent muscles were placed in sterile Mesenchymal Stem Cell Medium (MSCM; Sciencell, USA), and several flushes of MSCM were injected into the femurs using a 2-mL syringe. Then, mononuclear cells were separated from the marrow obtained by density gradient centrifugation with HISTOPAQUE-1077 (Sigma, USA) and plated in 25-cm² flasks (CORNING, USA) at a density of 1×10^6 cells/mL. Nonadherent cells were removed after 36 h, and the medium was replaced every 2–3 days. When the MSCs became confluent, they were harvested and re-plated. The cells were expanded to passage 3 for further study.

Three groups of scaffold samples were cut into 1.2 cm × 1.2 cm rectangular samples and fixed in CellCrown inserts (Scaffdex, Finland). Before cell seeding, the scaffolds were sterilized by UV irradiation for 2 h and immersed in 70% ethanol for 4 h to obtain a hydrophilic surface. Then, the scaffolds were placed in 24-well cell culture plates and incubated overnight with MSCM. The MSCs were seeded at a density of 50,000 cells per scaffold and cultured at 37 °C in a humidified atmosphere of 5% CO₂ in air. The culture medium (MSCM) was changed every other day.

2.7. Cell proliferation

The viability of the MSCs on the scaffolds was determined using the commercially available Cell Counting Kit-8 (CCK-8; Dojindo Lab., Japan). Cell proliferation tests were conducted on days 1, 7, 14 and 28. The medium was collected from the 24-well cell culture plates at each time point, and fresh medium containing 10% CCK-8 was added and incubated for 2 h. The absorbance was then measured at 450 nm in a microplate reader (Model 550, Bio-Rad, USA).

A standard curve was constructed to calculate the cell number of the sample ($n=3$).

2.8. Cell morphology

After 7 days, the collected cellular scaffolds were rinsed with PBS and fixed in 4% paraformaldehyde for 30 min. The MSCs were permeabilized with 0.1% Triton X-100 (Sigma, USA). The actin filaments and nuclei of the MSCs were stained with rhodamine-labeled phalloidin (Invitrogen, USA) and 4',6'-diamidino-2-phenylindole hydrochloride (DAPI; Invitrogen, USA), respectively. Images of the specimens were acquired with a laser scanning confocal microscope (LSCM; TCS SP5, Leica, Germany).

2.9. Histology

After 7, 14 and 28 days of post-seeding, cellular scaffolds were collected for histological analyses. Samples were rinsed with PBS and placed in 4% paraformaldehyde overnight. After dehydration, the samples were embedded in paraffin blocks. Cross sections were stained with hematoxylin and eosin (HE) and observed under an optical microscope (Eclipse E600, Nikon, Japan).

2.10. Statistical analysis

All quantitative data are presented as the mean ± standard deviation (SD). One-way analysis of variance was used to determine statistically significant differences ($p < 0.05$) between groups. All statistical analyses were performed using SPSS Statistics version 21.0 (IBM, USA).

3. Results

3.1. Electrospun scaffold morphology

The surface morphologies and cross-sectional structures of the random nanofibrous scaffold, aligned nanofibrous scaffold and NRS are shown in Fig. 2. The images of the NRS (Fig. 2G and H) revealed that the scaffolds were composed of random nanofibers and aligned nanoyarns. The NRS exhibited a three-dimensional porous structure, while the random (Fig. 2A and B) and aligned (Fig. 2D and E) nanofibrous scaffold comprised densely packed nanofibers. The nanofibers in the random nanofibrous scaffold exhibited a wide fiber alignment distribution (Fig. 2C). By contrast, most of the nanofibers in the aligned nanofibrous scaffold (Fig. 2F) and all of the nanoyarns in the NRS (Fig. 2I) formed angles ranging from 0° to 20°. The nanofiber diameters of the random nanofibrous scaffold (890.93 ± 192.25 nm) and NRS (868.94 ± 227.63 nm) were similar, whereas the aligned nanofibrous scaffold had statistically smaller fiber diameters (749.67 ± 148.11 nm). In addition, the nanoyarn diameter of the NRS was significantly (30.56 ± 6.32 μm) larger than the nanofibers in the nanofibrous scaffold.

As shown in Fig. 3A, the NRS had a mean pore size of 551.41 ± 472.70 μm², considerably larger than that of the random (72.8 ± 52.6 μm²) and aligned nanofibrous scaffolds (16.7 ± 11.9 μm²). In addition, the NRS exhibited a significantly higher porosity (Fig. 3B) of $79.2 \pm 3.2\%$ compared with the random ($75.1 \pm 1.7\%$) and aligned nanofibrous scaffolds ($73.6 \pm 2.1\%$).

3.2. Mechanical properties of electrospun scaffolds

The fiber alignment and overall scaffold structure had a profound effect on the mechanical properties of the scaffolds (Fig. 4). For the aligned nanofibrous scaffold and the NRS, Young's modulus in the direction parallel to the rotation of the mandrel was at least

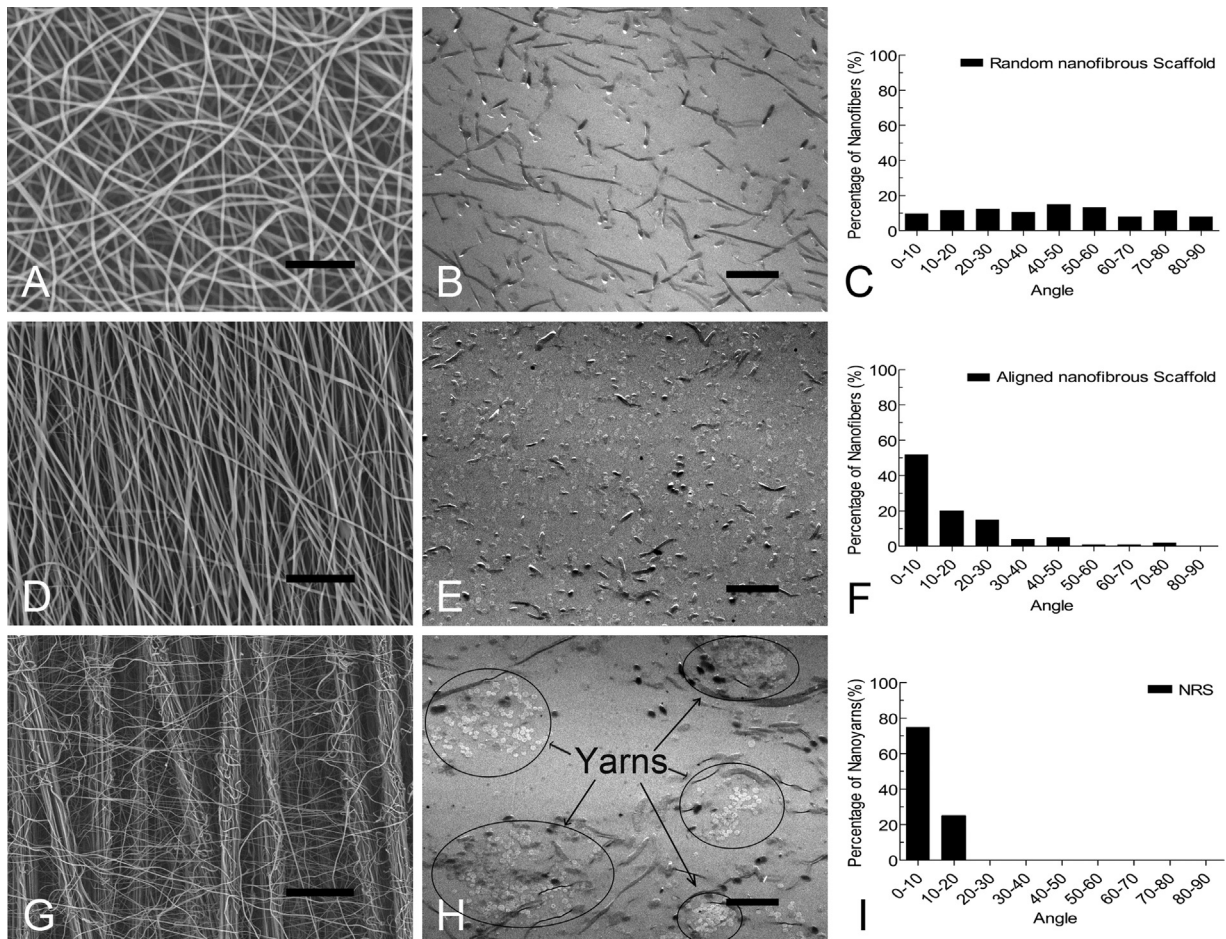


Fig. 2. Scanning ((A), (D), and (G)) and transmission ((B), (E), and (H)) electron microscopic images of the electrospun SF/P(LLA-CL) random nanofibrous scaffold ((A) and (B)), aligned nanofibrous scaffold ((D) and (E)), and NRS ((G) and (H)). Images ((E) and (H)) indicate that the yarns are twisted by aligned nanofibers in the NRS (scale bars: 20 μm for (A) and (D); 100 μm for (G); 10 μm for (B), (E) and (H)). Histograms ((C), (F) and (I)) represent the angular distribution of the nanofibers in the random and aligned nanofibrous scaffold and the nanoyarns in the NRS.

14 and 8 times greater than that in the perpendicular direction (433.56 ± 48.06 MPa vs. 29.72 ± 1.88 MPa and 288.95 ± 13.26 MPa vs. 32.51 ± 2.02 MPa, respectively). Similarly, a 10-fold increase in the tensile strength in the parallel direction compared to the perpendicular direction was observed in the aligned nanofibrous scaffold (39.10 ± 2.89 MPa vs. 3.44 ± 0.21 MPa), and a 5-fold increase was observed in NRS (24.25 ± 0.76 MPa vs. 4.43 ± 0.26 MPa). However, the elongation at break values of the aligned nanofibrous scaffold and the NRS in the parallel direction were significantly smaller than those in the perpendicular direction ($58.78 \pm 9.12\%$ vs. $212.18 \pm 10.15\%$ and $40.82 \pm 1.40\%$ vs. $162.76 \pm 10.52\%$). Because there were significant differences in the

mechanical properties in the parallel and perpendicular directions, both the aligned nanofibrous scaffold and NRS exhibited notable anisotropic mechanical properties. The random nanofibrous scaffold had the lowest tensile strength (9.70 ± 0.51 MPa) and Young's modulus (186.65 ± 8.87 MPa) but the highest elongation at break ($119.58 \pm 15.34\%$) compared with the aligned nanofibrous scaffold and NRS in the parallel direction. The Young's modulus value (Fig. 4B) of the aligned nanofibrous scaffold was approximately three times that of the random nanofibrous scaffold. The Young's modulus value of the NRS was lower than that of the aligned nanofibrous scaffold but was approximately two times that of the random nanofibrous scaffold. The tensile strengths (Fig. 4A) of the NRS and

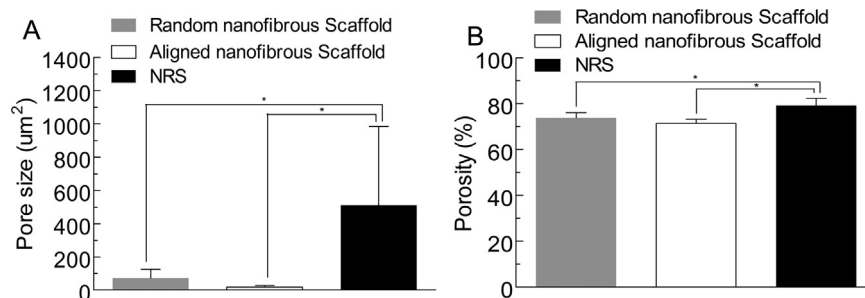


Fig. 3. Histograms (A) and (B) represent the pore size and the porosity of the random nanofibrous scaffold, aligned nanofibrous scaffold and NRS. The data are expressed as the mean \pm standard deviation (SD). The samples marked with (*) had a statistically significant difference between the two groups ($p < 0.05$).

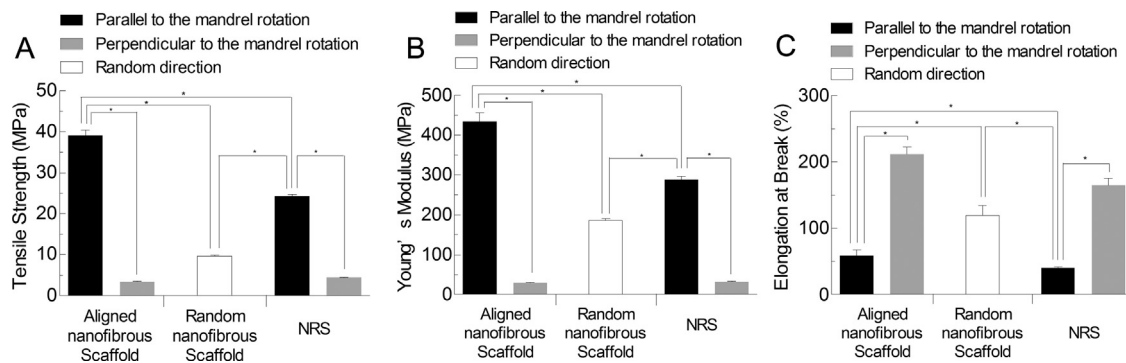


Fig. 4. The tensile strengths (A), Young's modulus values (B) and elongation at break values (C) of the SF/P(LLA-CL) aligned nanofibrous scaffold, random nanofibrous scaffold and NRS. The tests were performed in parallel and perpendicular to the mandrel rotating direction for the aligned nanofibrous scaffolds and NRSs. The mechanical tests were performed in a haphazard direction for the random nanofibrous scaffolds. Young's modulus was determined by regression of the linear portion of the stress–strain curve. Data are expressed as the mean \pm SD. The samples marked with (*) had a significant difference between the two groups ($p < 0.05$).

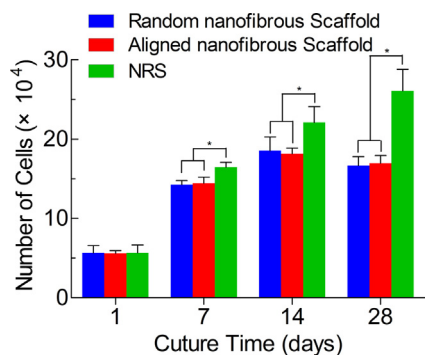


Fig. 5. CCK-8 result of MSCs cultured on the random nanofibrous scaffolds, aligned nanofibrous scaffolds and NRSs for up to 28 days. The data are expressed as the mean \pm SD. The samples marked with (*) had a significant difference between the two groups ($p < 0.05$).

aligned nanofibrous scaffold were significantly higher than that of the random nanofibrous scaffold.

3.3. Cell proliferation

A CCK-8 assay was utilized to evaluate the proliferation of MSCs on the three types of scaffolds for up to 28 days. The results shown in Fig. 5 indicate that there was no significant difference in the number of cells between the groups after 1 day of culture. Intriguingly, the number of cells on the random and aligned nanofibrous scaffolds increased from day 1 to day 14 and remained constant at day 28, whereas the number of cells on the NRS continued to increase up to day 28. In addition, the cell proliferation rate on the NRS was significantly higher than those on the random and aligned nanofibrous scaffolds at days 7, 14 and 28. There was no significant difference in the number of cells on the random and aligned nanofibrous scaffolds at each time point.

3.4. Cell morphology imaged by LSCM

MSCs grown on the scaffold samples were stained with rhodamine-labeled phalloidin and DAPI, and confocal sections were acquired using a LSCM. After a 7-day culture, the MSCs elongated along a particular direction when seeded on the aligned nanofibrous scaffold (Fig. 6B). Furthermore, aligned actin filaments were observed parallel to the axis of cell elongation. Cells were randomly distributed when seeded on the random nanofibrous scaffold (Fig. 6A) and exhibited a pyramidal morphology with randomly oriented actin filaments. The MSCs on the NRS (Fig. 6C) exhibited different morphological patterns depending on the cell

localization. Some cells were elongated and evenly spread on the nanoyarns, whereas others were randomly distributed between the nanoyarns.

3.5. Cell infiltration

To evaluate the extent of cell migration into the scaffolds, MSCs were seeded on the surfaces of three types of scaffolds for up to 28 days. HE-stained images of the cell-seeded scaffold cross sections are shown in Fig. 7. After a 7-day culture, the MSCs infiltrated to a depth of approximately 150 μ m from the surface of the NRS (Fig. 7G). By day 14, an increase in the number of infiltrated cells and nearly half-depth (approximately 300 μ m) cell ingrowth were observed (Fig. 7H). In addition, after a 28-day culture, the MSCs had migrated to a depth of approximately 500 μ m in the NRS (Fig. 7I). By contrast, cell migration to a depth of approximately 40 μ m was observed in the random nanofibrous scaffolds after a 28-day culture (Fig. 7C). No obvious cell infiltration was observed in the aligned nanofibrous scaffolds during the entire culture period (Fig. 7D–F).

4. Discussion

Electrospinning has been widely investigated for fabricating nanofibrous tissue engineering scaffolds. By changing the processing parameters [20], the morphology and orientation of the electrospun fibers can be controlled. When collected on a high-speed rotating mandrel, the nanofibers are aligned during deposition and possess anisotropic mechanical properties similar to those of tendons. However, these aligned nanofibrous scaffolds are only useful for in vitro studies because they cannot form the 3D architectures necessary to replicate native tissues [21]. Yarns twisted by a bundle of axially oriented electrospun nanofibers represent another type of aligned structure. Electrospun nanoyarns are expected to provide new opportunities for the development of well-defined 3D nanofibrous structures with enhanced functions and better mechanical performance [22]. In the present study, we introduced a novel aligned nanoyarn-reinforced nanofibrous scaffold for tendon tissue regeneration.

As shown in Fig. 2D–I, the SF/P(LLA-CL) aligned nanofibrous scaffold and NRS exhibited highly oriented structures. The aligned microscale yarns twisted by nanoscale fibers in the NRS were similar in structure and organization to the highly oriented collagen fiber bundles of native ECM. The aligned yarns and random nanofibers of the NRS provided a 3D structure with larger pores and greater porosity (Fig. 3). These properties would provide more space for cell adhesion and migration, and thus the NRS should

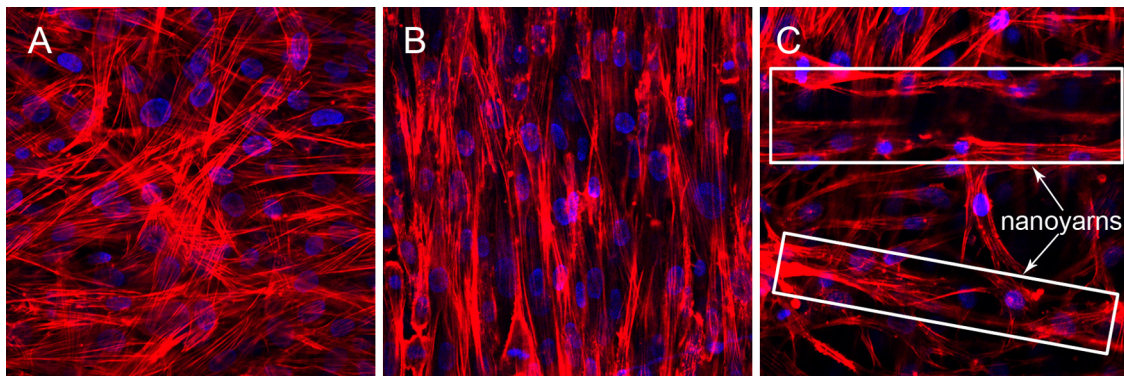


Fig. 6. Confocal microscopy fluorescence images show the actin filaments (red) and nuclei (blue) of MSCs on the random nanofibrous scaffold (A), aligned nanofibrous scaffold (B) and NRS (C) after 7-day culture. Magnifications of all images are 400 \times . (For interpretation of the references to color in this figure legend, the reader is referred to the web version of this article.)

enable more efficient nutrient and oxygen delivery and metabolite elimination.

MSCs obtained from rats were seeded onto the three different types of electrospun scaffolds and cultured for up to 28 days. According to the CCK-8 cell proliferation assay (Fig. 5), all scaffolds were capable of supporting cell proliferation in vitro. The number of MSCs on the random and aligned nanofibrous scaffolds increased from day 1 to day 14 and remained constant up to day 28, indicating that the number of cells reached the maximum value after 14 days of culture. By contrast, the number of cells on the NRS increased throughout the entire culture period.

Furthermore, the cell proliferation rate on the NRS was significantly higher than those on the random and aligned nanofibrous scaffolds at days 14 and 28, indicating that the NRS provided a more favorable environment for cell proliferation, most likely due to its higher porosity. After migrating into the NRS, the MSCs exhibited a 3D culture pattern, with more space for proliferation. The random and aligned nanofibrous scaffolds permitted limited cell infiltration, and therefore only the surfaces of the scaffolds were utilized for cell proliferation.

The structure and orientation of the nanofibers greatly influenced the positioning and alignment of cells. The cells were

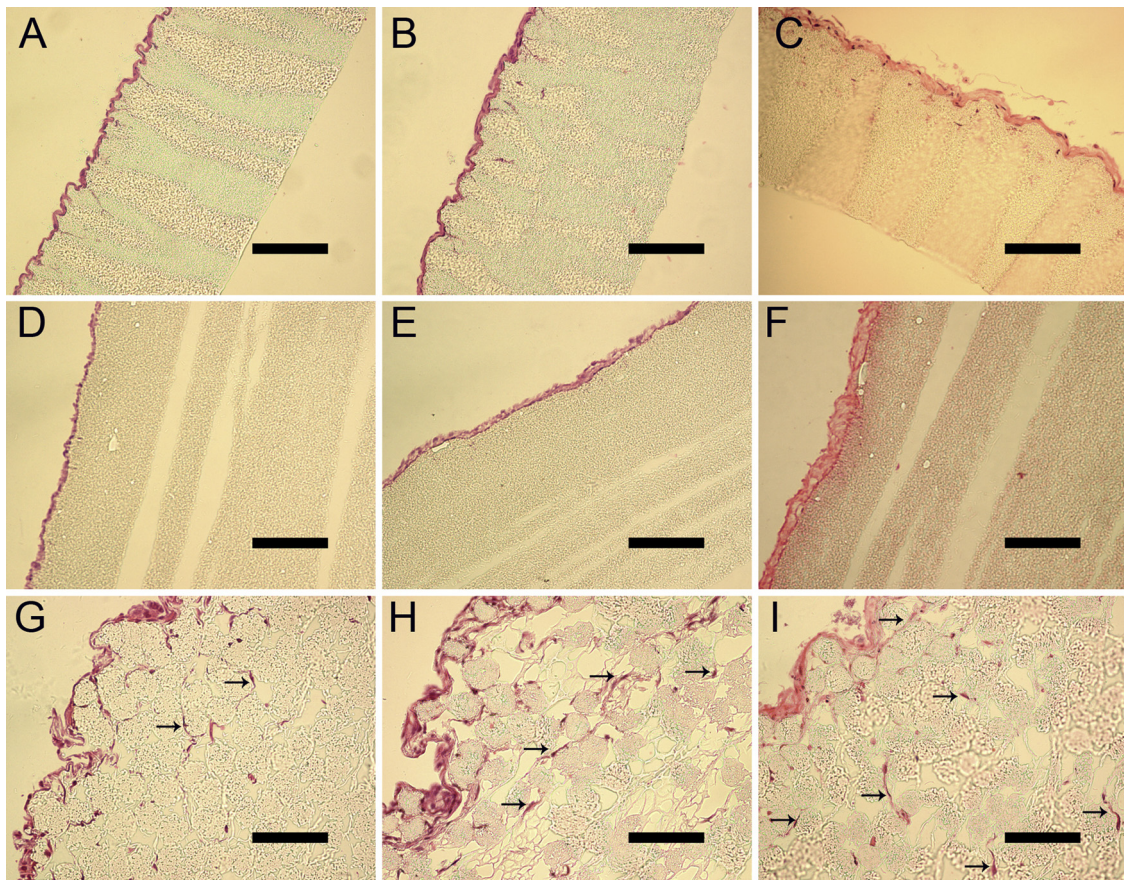


Fig. 7. HE-stained histology images show MSCs interactions with the random nanofibrous scaffolds ((A)–(C)), aligned nanofibrous scaffolds ((D)–(F)) and NRS ((G)–(I)) at days 7 ((A), (D) and (G)), 14 ((B), (E) and (H)) and 28 ((C), (F) and (I)). The MSCs (black arrow) infiltrated to a depth of approximately 150 μm from the surface of the NRSs at day 7 (G), approximately 300 μm at day 14 (H) and approximately 500 μm at day 28 (I). By contrast, images show that cell infiltration is limited on the random nanofibrous scaffolds ((A)–(C)) and aligned nanofibrous scaffolds ((D)–(F)) during the entire culture period. Scale bars: 100 μm for all images.

randomly spread when cultured on the random nanofibrous scaffolds. However, the cells were highly evenly distributed and elongated along the direction of the fibers on the aligned nanofibrous scaffold. Interestingly, the MSCs on the NRSs exhibited an aligned and elongated growth pattern along the nanoyarns but were diversely distributed among the yarns. These results indicate that the fiber features may modulate cell migration, morphology and cytoskeleton organization, in agreement with previous studies [9,10,13,21].

To ensure successful engineering graft for clinical applications, the electrospun scaffold must provide acceptable mechanical strength. The tensile strengths of adult human ligaments and tendons are 4.4 to 660 MPa, and the elastic modulus value is 200–1500 MPa [23–25]. The aligned nanofibrous scaffold exhibited the strongest mechanical properties when pulled along the fibrous direction. The tensile strength was more than 4 times greater and the Young's modulus value was approximately 3 times greater (Fig. 4A and B) than those of the random nanofibrous scaffolds. This trend is consistent with the results of previous studies [10,21]. Although the aligned nanofibrous scaffold shows promise for tendon tissue engineering, some limitations remain. The major limitation is that cell infiltration into the aligned nanofibrous scaffold is limited due in part to the dense fiber packing, which was also observed in the random nanofibrous scaffold [26]. To address this problem, we introduced the novel 3D aligned NRS. Although not as strong as the aligned nanofibrous scaffold, the NRS exhibited superior mechanical performance compared to the random nanofibrous scaffold (Fig. 4). The structure of the aligned nanoyarns in the scaffold contributes to the improvement in the tensile properties. In addition, the NRS provides larger pores and sufficient space for cell infiltration. Histological examination (Fig. 7) revealed that only one cell sheet formed on the surface of the aligned and random nanofibrous scaffolds after up to 28 days of culture, whereas the MSCs infiltrated to a depth of approximately 500 μm in the NRS. In this respect, the NRS is the most advantageous among the three types of scaffolds in terms of cell infiltration and provides adequate mechanical support for functional applications in vivo.

Previous studies [11,27] have noted that fibrous scaffolds with high porosities promote cell proliferation and infiltration at the cost of decreased mechanical properties. Wu [12] and Xu [13] fabricated porous nanoyarn scaffolds via dynamic liquid electrospinning. Their scaffolds had a larger pore size (approximately 637.94 μm^2) and higher porosity (approximately 85%) and were beneficial for cell infiltration. However, the mechanical strength of the nanoyarn scaffolds was considerably weaker than that of the random nanofibrous scaffolds and thus may not satisfy the mechanical requirements for tendon tissue engineering. In the present study, we fabricated the NRS and attempted to obtain a balance between the porosity and mechanical properties of electrospun scaffolds. This novel scaffold had excellent mechanical strength and a porous structure, which is beneficial for cell proliferation and infiltration. However, the cell density in the NRS was non-uniform; the seeding region contained more cells than the internal portion (Fig. 7G–I). An uneven distribution of cells was also observed when scaffolds were engineered to promote infiltration [11]. This uneven distribution might be the result of static culture after surface seeding, which is the most common method for populating scaffolds with cells [9]. Previous studies [28,29] have indicated that the ability of cells to move through layers of nanofibers is limited in the static state. In subsequent studies, these limitations might be overcome through the use of perfusion or dynamic culture conditions. Overall, the NRS has sufficient porosity for the delivery of nutrients and for cell migration and has potential as a substitute in tissue engineering applications for tendon repair.

5. Conclusions

A novel 3D SF/P(LLA-CL) scaffold composed of aligned nanoyarns and random nanofibers was fabricated via electrospinning using a two-collector system. These scaffolds exhibited higher porosity than SF/P(LLA-CL) random and aligned nanofibrous scaffolds. Biocompatibility analysis demonstrated that the NRS yielded improved cell proliferation regulated cell morphology. More remarkably, the 3D structure of the NRS enabled cell infiltration. In addition, the NRS exhibited increased mechanical strength in the direction parallel to the nanoyarns. This study indicates that the NRS represents a balance between porosity and mechanical properties to satisfy the requirements for tendon tissue engineering applications.

Acknowledgements

This work was financially supported by the National Natural Science Foundation of China (Grant no. 31271035), the Shanghai Committee of Science and Technology (Grant no. 11nm0506200), and the National High Technology Research and Development Program of the Science and Technology Ministry of China (863 Program, Grant no. 2013AA032203).

References

- [1] P.X. Ma, *Adv. Drug Delivery Rev.* 60 (2008) 184.
- [2] L. Jin, T. Wang, M.L. Zhu, M.K. Leach, Y.I. Naim, J.M. Corey, Z.Q. Feng, Q. Jiang, *J. Biomed. Nanotechnol.* 8 (2012) 1.
- [3] J. Riesle, A.P. Hollander, R. Langer, L.E. Freed, G. Vunjak-Novakovic, *J. Cell. Biochem.* 71 (1998) 313.
- [4] W.J. Li, C.T. Laurencin, E.J. Caterson, R.S. Tuan, F.K. Ko, *J. Biomed. Mater. Res.* 60 (2002) 613.
- [5] K. Zhang, H. Wang, C. Huang, Y. Su, X. Mo, Y. Ikada, *J. Biomed. Mater. Res. A* 93 (2010) 984.
- [6] R.L. Mauck, B.M. Baker, N.L. Nerurkar, J.A. Burdick, W.J. Li, R.S. Tuan, D.M. Elliott, *Tissue Eng. B* 15 (2009) 171.
- [7] M.E. Frohbergh, A. Katsman, G.P. Botta, P. Lazarovici, C.L. Schauer, U.G. Wegst, P.I. Lelkes, *Biomaterials* 33 (2012) 9167.
- [8] W.L.J. Bao, Y.D.Y. Sun, *J. Mater. Sci.* 48 (2013) 4223.
- [9] B.M. Baker, A.M. Handorf, L.C. Ionescu, W.J. Li, R.L. Mauck, *Expert Rev. Med. Devices* 6 (2009) 515.
- [10] W.J. Li, R.L. Mauck, J.A. Cooper, X. Yuan, R.S. Tuan, *J. Biomech.* 40 (2007) 1686.
- [11] B.M. Baker, A.O. Gee, R.B. Metter, A.S. Nathan, R.A. Marklein, J.A. Burdick, R.L. Mauck, *Biomaterials* 29 (2008) 2348.
- [12] J.L. Wu, S. Liu, L.P. He, H.S. Wang, C.L. He, C.Y. Fan, X.M. Mo, *Mater. Lett.* 89 (2012) 146.
- [13] Y. Xu, J. Wu, H. Wang, H. Li, N. Di, L. Song, S. Li, D. Li, Y. Xiang, W. Liu, X. Mo, Q. Zhou, *Tissue Eng. C* 19 (2013) 925.
- [14] X.M. Mo, C.Y. Xu, M. Kotaki, S. Ramakrishna, *Biomaterials* 25 (2004) 1883.
- [15] C. Vaquette, C. Kahn, C. Frochet, C. Nouvel, J.L. Six, N. De Isla, L.H. Luo, J. Cooper-White, R. Rahouadj, X. Wang, *J. Biomed. Mater. Res. A* 94 (2010) 1270.
- [16] C. Zeng, Q. Yang, M. Zhu, L. Du, J. Zhang, X. Ma, B. Xu, L. Wang, *Mater. Sci. Eng., C* 37 (2014) 232.
- [17] A.F. Lotus, E.T. Bender, E.A. Evans, R.D. Ramsier, D.H. Reneker, G.G. Chase, *J. Appl. Phys.* 103 (2008) 024910, <http://dx.doi.org/10.1063/1.2831362>.
- [18] D.S. Zhang, M. Luo, D.D. Arola, *Opt. Eng.* 45 (2006) 033605, <http://dx.doi.org/10.1117/1.2182108>.
- [19] Q. Tan, P.P. Lui, Y.F. Rui, Y.M. Wong, *Tissue Eng. A* 18 (2012) 840.
- [20] W. Liu, S. Thomopoulos, Y. Xia, *Adv. Healthcare Mater.* 1 (2012) 10.
- [21] L.A. Bosworth, N. Alam, J.K. Wong, S. Downes, *J. Mater. Sci.: Mater. Med.* 24 (2013) 1605.
- [22] U. Ali, Y. Zhou, X. Wang, T. Lin, *J. Text. Inst.* 103 (2012) 80.
- [23] G.A. Johnson, D.M. Tramaglino, R.E. Levine, K. Ohno, N.Y. Choi, S.L. Woo, *J. Orthop. Res.* 12 (1994) 796.
- [24] T.A. Wren, S.A. Yerby, G.S. Beaupre, D.R. Carter, *Clin. Biomech. (Bristol, Avon)* 16 (2001) 245.
- [25] R.B. Swenson, P. Hansen, T. Hassenkam, B.T. Haraldsson, P. Aagaard, V. Kovanen, M. Krogsgaard, M. Kjaer, S.P. Magnusson, *J. Appl. Physiol.* 112 (2012) 419–426.
- [26] C. Gualandi, M. Govoni, L. Foroni, S. Valente, M. Bianchi, E. Giordano, G. Pasquinelli, F. Biscarini, M.L. Focarete, *Eur. Polym. J.* 48 (2012) 2008.
- [27] S. Zhong, Y. Zhang, C.T. Lim, *Tissue Eng. B* 18 (2012) 77.
- [28] Q.P. Pham, U. Sharma, A.G. Mikos, *Biomacromolecules* 7 (2006) 2796.
- [29] N.L. Nerurkar, S. Sen, B.M. Baker, D.M. Elliott, R.L. Mauck, *Acta Biomater.* 7 (2011) 485.